Dose-Response:
An International Journal
July-September 2020:1-9

DOI: 10.1177/1559325820917836
journals.sagepub.com/home/dos
SAGE

Lactoferrin-Loaded PEG/PLA Block Copolymer Targeted With Anti-Transferrin Receptor Antibodies for Alzheimer Disease

Guichen Li[1], Xianghong Sun[2], Xiaona Wan[2], and Dongming Wang[2]

Abstract

Last few years, struggles have been reported to develop the nanovesicles for drug delivery via the brain–blood barrier (BBB). Novel drugs, for instance, iAβ_5, are efficient to inhibit the aggregates connected to the treatment of Alzheimer disease and are being evaluated, but most of the reports reflect some drawbacks of the drugs to reach the brain in preferred concentrations owing to the less BBB penetrability of the surface dimensions. In this report, we designed and developed a new approach to enhance the transport of drug via BBB, constructed with lactoferrin (Lf)-coated polyethylene glycol-polylactide nanoparticles (Lf-PPN) with superficial monoclonal antibody-functionalized antitransferrin receptor and anti-Aβ to deliver the iAβ_5 hooked on the brain. The porcine brain capillary endothelial cells were utilized as BBB typically to examine the framework efficacy and toxicity. The cellular uptake of the immuno-nanoparticles with measured conveyance of the iAβ_5 peptide was significantly enhanced and associated with Lf-PPN without monoclonal antibody functionalizations.

Keywords

immune nanoparticles, blood–brain barrier (BBB), Alzheimer disease, therapeutic peptides, drug delivery systems

Introduction

Alzheimer disease (AD) is one of the types of dementia, presently demonstrating immediate medical uses. The actual preclinical treatment, such as the *N*-methyl-D-aspartate receptor and acetylcholinesterase inhibitors, only offers fleeting suggestive respite, with small effects on reducing the development of the disorder. Therefore, the establishment of new therapy for AD is important.[1-4] Alzheimer disease is considered pathologically through the age-related amyloid-beta (Aβ) admission, neurofibrillary masses, synapses, and neuronal damage. Aberrant accumulation of Aβ, especially its 42 amino acid isoforms (Aβ42), is the essential pathogenic mechanism of AD. The Aβ derived from the amyloid precursor protein via cleavage through the BACE1 expression ratios. Therefore, developing drug delivery strategies across the blood–brain barrier (BBB) is important for therapeutic purposes.[5-9]

Lactoferrin (Lf) is a human cationic iron (Fe) that binds with glycoprotein belonging to the transferrin (Tf) group. It has numerous biological functions such as intense antimicrobial, immunomodulatory, and anti-inflammatory functions. Lactoferrin receptors are creating the BBB of various types and help in the delivery of Lf through the BBB in vivo and in vitro.[10-13] There are 2 classes of binding sites for Lf on cell membrane, a high affinity 105 kDa receptor protein and the low-affinity glycosaminoglycan-binding sites. More recently, the establishment of the brain cell uptake of Lf was much developed by Tf and OX26. Moreover, Hu et al report the Lf as brain target the cellular membrane for the efficient brain transporter.[14] The outcome of Lf is the potential target molecule for enhancing brain delivery.[15-18]

Amyloid-beta peptide (Aβ) contains the 42 amino acids and the vital fundamental signs of AD. The action of the

[1] Department of Clinical Psychology, Qingdao Mental Health Center, Qingdao, China
[2] Second Elderly Ward, Qingdao Mental Health Center, Qingdao, China

Received 20 January 2020; received revised 19 February 2020; accepted 25 February 2020

Corresponding Author:
Dongming Wang, No. 299, Nanjing Road, North District 266034, Qingdao, China.
Email: dongming_wang@yahoo.com

peptides in the brain parenchyma outcomes in the neuronal damage has been connected. The Aβ derivatives from the proteolytic bond cleavage of the amyloid protein, on the membrane protein.[19-21] The presence of Aβ in the brain depends on peptide's production, degradation, and aggregation, which is a concentration-dependent process. Numerous reports recommend that the confirmation transition from the random coil/α-helix model to the β-helix sheets favors the Aβ aggregations. The exact invent to avoid this method could be reconversation of Aβ confirmations.[22-24] These methods can be endorsed through adding new components that are able to estimate the β-sheet confirmations out of the equilibrium; up to date, some of the small molecules that are synthesized inhibited and reduced the Aβ aggregations.[25-27] The core peptide residues of Aβ hydrophilic peptides are 17 to 21 and 30 to 42 which have been connected to the aggregation methods, so that 17 to 21 residues inhibit similar degree of the hydrophobic environments yet have a very less ratio to adopt the β-sheet confirmations.[28-30]

From the recent reports, Shyam et al described the linear polyethylene glycol polymer-based micelles nanocomposition frame of BACE1 in the brain via infusing the nanocomposition in mouse lateral ventricle.[31] However, the nanocomposition meets various clinical strategies for the translation, for example, invasive administration protocols or risk of the immune or inflammatory actions.[32-34] Recently, the rabies virus glycol as a brain target ligations altered on the surface of the small interfering RNA (siRNA) drug delivery through the trimethylated chitosan, exosome, and delivery of the BACE1 siRNA to mice brain injections. Henceforth, for the BACE inhibition, only enhancing BBB is inadequate. BACE is the important β-secretase in vivo with different substances and its level is very high in central neuron. So, in order to enhance the safety and efficiency of RNA interference, the genes have to be the particular delivery for neurons.[35-37] Xinguo research groups demonstrated the phage-showing l-peptide TGNY-KALHPHNG (represented as TGNK) facilitates PEG-poly-lactic-co-glycolic acid (PLGA) nanocomposition through the BBB, leading to remarkable brain accumulations.[38] The same research groups developed CG peptide (D-CGNHPHLAKYNGT), the retro-isomerization of the TGN, which shows the high target brain accumulations of TGNK.

In spite of these advancements, we have developed the Lf-conjugated PEG-polylactide (PLA) nanoparticles (PPN) for AD delivery systems. The Lf-PPN was used as the drug-loading transporter due to its biocompatibility over the PEG-PLA nanoparticles. The Lf-PPN nanoparticles with monoclonal antibodies (mAbs) for BBB receptors for endogenous and mAbs for Aβ aggregates peptides. The exact antibody OX26 was used across the BBB cell lines. The mAb with DE2B4 for Aβ could be utilized to deliver the immuno-nanoparticles to the medication transporter for the β-sheet breakdown peptides to straight deposits of the Aβ.

Materials and Methods

Synthesis of Lf-Loaded Nanoparticles

The Lf-loaded polymer nanoparticles were prepared by the nanoprecipitation protocol.[39-42] Concisely, $mPEG_{5000}$-PLA_{16000} (50 mg) and the Lf (5 mg) were immersed into the DCM and added dropwise to the 20 mL of DD water with magnetic stirring, which obtained polymeric concentration of 1 mg/mL. After magnetic stirring for 1 hour, the residual organic solvent was removed using the rotary evaporation methods under low pressure. The solution containing polymeric nanoparticles was filtered using centrifugal filter machine and cleaned using DD water.

Characterization and Size Determination

The hydrodynamic diameters (D_H), Z potential, and polydispersity index (PDI) of the Lf-loaded polymeric nanoparticles were evaluated by the dynamic light scattering (DLS) method using the Nano-ZS90, Malvern, at 30°C. The transmission electron microscopy (TEM) analysis images were used to examine the TECNAL 10. The Lf-PPN at the concentration of 1 mg/mL was placed into the 3 K mesh copper grid covered with carbon. Almost 3 minutes after the admission, the water was removed from the surface using the filter paper and then lyophilized. The positive discoloration was achieved by 2% uranyl acetate aqueous solution.

Cytotoxicity Examination of the Cells

The porcine brain capillary endothelial cells (PBCECs) and C6 glioma cells were obtained from the brains according to the previously reported protocol. The cells were cultivated in the 96-well chamber and maintained by the plating media (the medium contains l-glutamine 1 mM, 1% penicillin, and 1% of gentamycin) at 37°C with humidified environment comprising 5% of CO_2 incubation. The cellular uptake examinations and the cytotoxicity assay were evaluated from these cells.

Entrapment Efficiency to Examine the β-Sheet Breakdown Peptide

The centrifugations of Lf-PPN suspensions of supernatant solutions harvested and evaluated the encapsulated efficacy of $iA\beta_5$ peptide by analyzing the microplate reader using 570 nm emission and 480 nm excitations.[43-47]

Controlled Release From the Lf-PPN

The release profiles of total $iA\beta_5$ peptide-loaded Lf-PPN were determined by dialysis using a membrane; 10 mL of the nanocomposition solution was dialyzed against 50 mL of phosphate buffer. At programmed time intermissions, the release media (1 mL) were composed and the fresh media (1 mL) were accompanied. The aggregates of released peptide were measured to the

dialysis baggage. Finally, the peptide ratios were calculated using the reported protocol.

Cellular Uptake Assay

The Lf-PPN cellular uptake was examined by fluorescence microscopy. The synthesized cellular uptake was loaded with the iAβ_5 peptide. The PBCECs were incubated in the same medium, and after 24-hour examination of incubation, the cell culture medium was changed. Usually, the monolayer confluence of the cells was reached after 3 days at 5×10^5 cells per each well. Last day, the cell culture medium was changed and added with various concentrations of Lf-PPN. The Lf-PPN was incubated with different time intervals and later washed with Lf-PPN via aspiration. The cells were harvested and washed with phosphate-buffered saline (PBS) 3 times; later, the acid pH buffer was added for 10 minutes, and subsequently, the cells were washed with PBS solution. The supernatants of the cells were lysed into 1% Triton for 1 hour at 70°C. Further, the cells were stirred and the Lf-PPN setup efficacy was examined through the fluorescence in the plate reader.[47-49]

Toxicity of the iAβ_5 Peptide-Loaded Lf-PPN

The iAβ_5 peptide-loaded Lf-PPN was incubated with PBCECs for 2 hours. Also, PBCECs were incubated without iAβ_5 peptide-loaded Lf-PPN and the cells were lysed using 1% triton. The PBCECs were incubated with the 40:1 percentage of Alamar-Blue reagents. Finally, the cell toxicity was examined by fluorimetry with 252 nm excitations and 575 nm emissions.

Hemolysis of Lf-PPN and Lf-PPN Conjugate With the mAb to the Tf Receptors

Freshly collected human blood samples were collected from the Department of Clinical Psychology, Qingdao Mental Health Center, Qingdao, China, and it was permitted by the ethical committee of the Department of Clinical Psychology, Qingdao Mental Health Center, Qingdao, China. We have conducted hemolysis according to the previously reported procedures. The blood was centrifuged and the supernatant solution was extracted and washed with cold PBS for 3 times fully eliminating the blood, thus yielding human red blood cells (hRBCs). Later, the hRBCs (0.1) were diluted with cold PBS. The solution was transferred to a 5-mL tube with 0.9 mL of DD water added, and it was used as a positive control. Further 0.9 mL was used as a negative control. Furthermore, this PBS-containing solutions Lf-PPN and Lf-PPN loaded mAbs (5 to 30 μg/mL), respectively. Later, this mixture was incubated for 3 hours, followed by centrifugation, and the absorbance was calculated by ultraviolet spectrometer using the general formula: $\%\ \text{Hemolysis} = (A_s - A_n)/(A_p - A_n) \times 100\%$, where, A_s, A_n, and A_p are the absorbance of the sample, the negative control, and the positive control, respectively.[50-53]

Statistical Analysis

The data are presented as mean $\pm$ standard deviation. The significance of the compared measurements was evaluated using 2-tailed unpaired Student t test. All analyses were performed with GraphPad Prism Statistics 17.0 ($^*P < .05$, $^{**}P < .01$).

Results and Discussions

Synthesis and Characterizations of Lf-PPN Conjugate With mAb to the Tf Receptors

The Lf-PPN was synthesized using nanoprecipitation methods by adding drug and polymer to the water.[54] Transmission electron microscopy analysis reveals the Lf-PPN displays well-organized spherical structure (Figure 1A). The physicochemical property of the Lf-PPN was examined after synthesis of each step, which is represented in Table 1. The mean diameter of the Lf-PPN was $\sim$90 and $\sim$68 nm in water and medium, respectively, with size and PDI of Lf-PPN (0.123 ± 0.05) showing the nanodispersion structures confirmed by the DLS analysis (Figure 1B). Furthermore, the presence of homodisperse populations of the nanoparticles was confirmed by hydrodynamic parameters (D_H) ranging from 90 to 95 nm. Additionally, we observed Lf-PPN for various days; Lf-PPN remains without precipitation after 7 days, which confirms the stability of Lf-PPN for long-time uses (Figure 1C). The diameter of nanoparticles less than 100 nm is activate for the passive in vivo tumors specific through the enhanced permeability and retention (EPR) effect and can attain the deep penetration of the solid tumors. In addition, as shown in Table 1, the Lf-PPN examined slight negative charge of the surface, as shown by the evaluations of Z potentials. These outcomes show the densely packed core shell structures forming different formulations with negatively charged nanoparticles. When these nanoparticles were kept in the room temperature with PBS solution for several days, no precipitation was detected.[55-57] These excellent outcomes triggered to explore in vitro analysis of AD.

Binding Affinity of the Lf-PPN Conjugate With the mAb to the Tf Receptors

Furthermore, the binding efficiency of the Lf-PPN conjugate with the mAb to the Tf receptors and to Aβ peptide was examined by ELISA. The Lf-PPN post mAb was used as the positive control. This Lf-PPN shows the remarkable absorbance at the range of 410 nm, when associated with the Lf-PPN conjugate with the mAb to the Tf receptors such as OX26 and DE2B4. These outcomes validate that the Lf-PPN conjugate with the mAb to the Tf receptors and the mAb binding affinity are conserved (OX26 binds with the mAb and DE2B4 binds with the Aβ peptides).

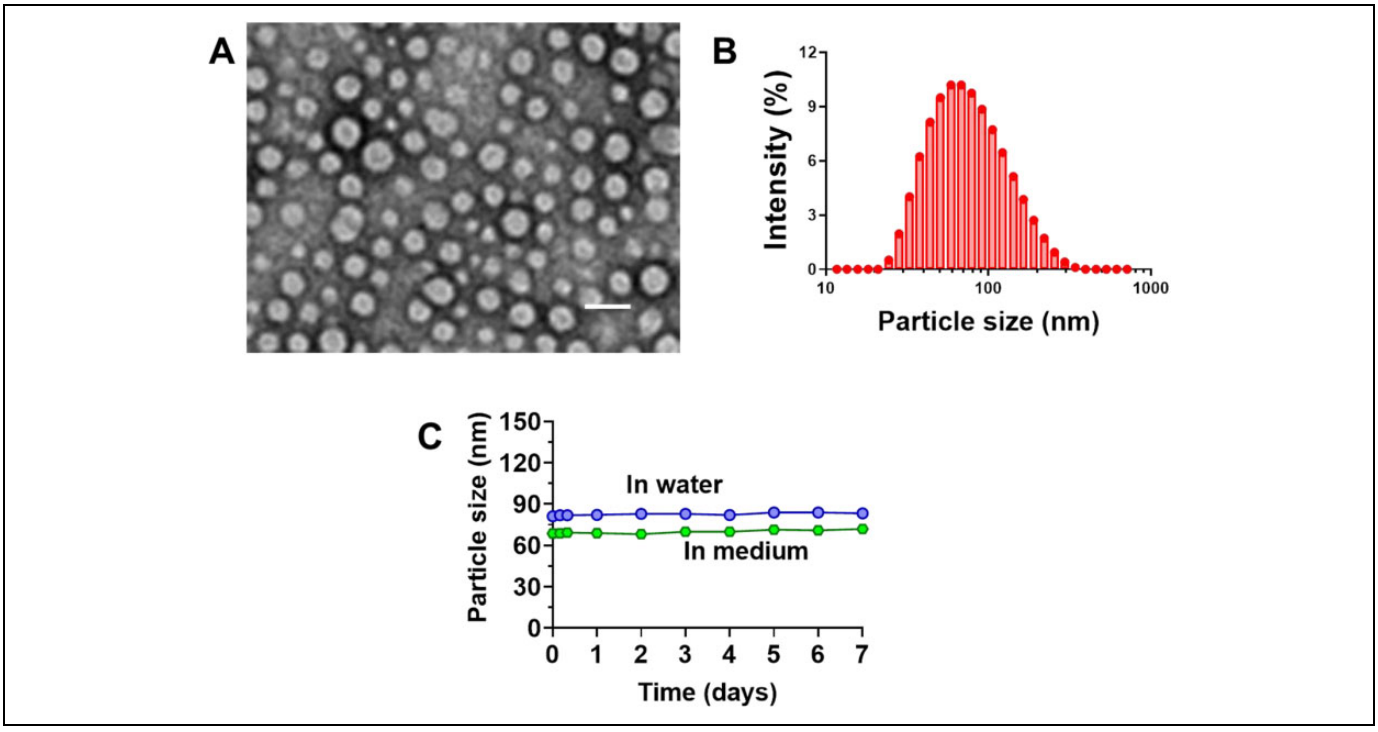

Figure 1. Characterization of Lf-PPN. A, The TEM analysis of Lf-PPN, scale bar 100 nm. B, The DLS analysis of Lf-PPN, which shows the average size of ~95 nm. C, The stability of the Lf-PPN with different days at the end of 7 days without changing the particle size. At end of the day, we didn't find any precipitation. DLS indicates dynamic light scattering; Lf-PPN, lactoferrin-coated PEG-PLA nanoparticles; TEM, transmission electron microscopy; PEG, polyethylene glycol; PLA, polylactide.

Table 1. Diameter and Polydispersity Index (PDI) of Lf-PPN With the Individual Standard Deviations.[a]

Nanoparticles	Diameter (nm)	PDI
Lf-PPN	95 ± 2.33	0.123 ± 0.05
Lf-PPN with OX26	128 ± 3.21	0.136 ± 0.06
Lf-PPN with DE2B4	132 ± 3.84	0.141 ± 0.04

Abbreviations: Lf-PPN, lactoferrin-coated PEG-PLA nanoparticles; PEG, polyethylene glycol; PLA, polylactide.
[a]n = 3.

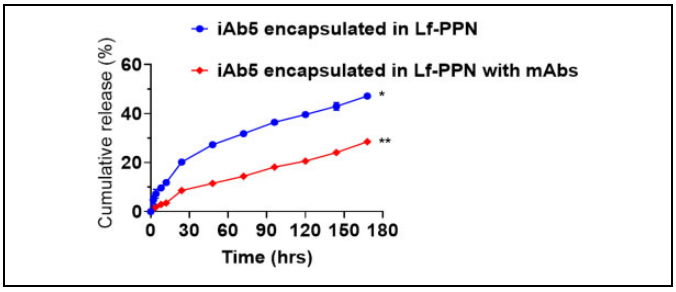

Figure 2. Entrapment efficiency to examine the β-sheet breakdown peptide. The in vitro cumulative release of iAb5 encapsulated Lf-PPN with and without mAbs at 37°C, pH 7.4 (*$P < .05$; **$P < .01$). Lf-PPN indicates lactoferrin-coated PEG-PLA nanoparticles; PEG, polyethylene glycol; PLA, polylactide.

Entrapment Efficiency to Examine the β-Sheet Breakdown Peptide

The efficiency of Lf-PPNs to deceive $iA\beta_5$ receptors is ~60% ± 10%. The controlled release of the Lf-PPNs plays a vital role in Lf-PPN size, solubility, degradations, and loaded drugs of the nanoparticle frameworks. The predictable results to confirm the drug release profile show the Aβ peptide-loaded Lf-PPN reserves an enhanced efficiency to the frameworks. In contrast, if the drug is not well entrapped, a fast and undesired premature release will occur. The slow degradation of PLGA polymers is mainly due to the matrix bulk degradation. In this degradation process, water intrusion leads to hydrolysis of the ester bonds. These methods lead to the production of shell pore that allows the release of drugs. Nevertheless, the controlled drug release is measured via physical and chemical properties concerning the Lf-PPN and the encapsulation properties of the drugs. These dialysis methods were utilized to examine the controlled release outcomes of the encapsulation in the Lf-PPN and associated with the free $iA\beta_5$ receptors. The controlled release was conducted in the PBS at pH of 7.2 at 37°C. The controlled release profiles of the Aβ peptide loaded in the Lf-PPN displayed the initial eruption in about 5 hours monitored via sluggish release for 6 days (Figure 2). In the first 10 hours, half percentage of the $iA\beta_5$ was released from the Lf-PPN. Then after 24 hours, a slow release was touched 40% to 50%. Later, the conjugation of Lf-PPN nanoparticles with the mAbs on the nanoparticle

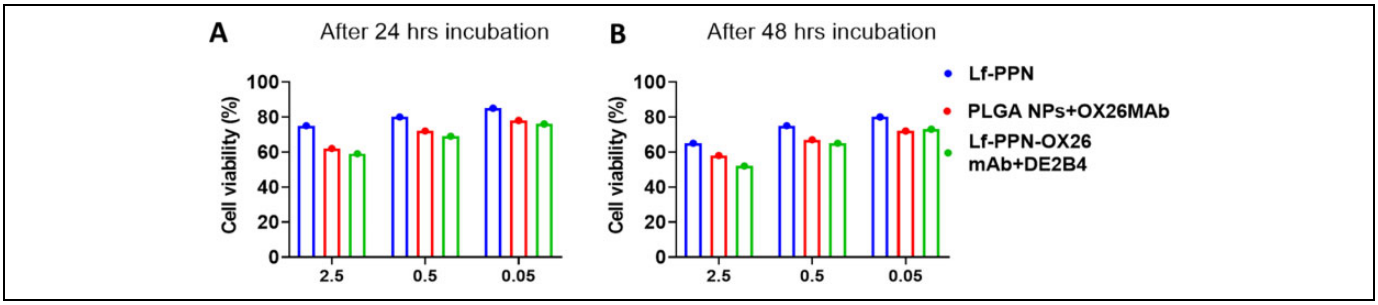

Figure 3. Cytotoxicity of Lf-PPN, Lf-PPN/OX26, and Lf-PPN/OX26+DE2B4 incubated with C6 glioma cells for (A) 24 hours, (B) 48 hours at 37°C. Lf-PPN indicates lactoferrin-coated PEG-PLA nanoparticles; PEG, polyethylene glycol; PLA, polylactide.

surface does not show without affecting the controlled release into the Lf-PPN and with mAbs was also examined, probably owing to the aqueous permeation effects via mAb, as previously reported.

Cytotoxicity of Nanoparticles Formulations

In vitro cytotoxicity of the model drug Lf-PPN formulated in the Lf-PPN/OX26 and Lf-PPN/OX26+DE2B4 conjugation nanoparticles on their surface was investigated with C6 glioma cells after 24 hours, then 48-hour incubation at 37°C, and the results are shown in Figure 3. Generally, 2 trends could be observed. First, the cytotoxicity of the drug formulated in the various nanoparticles increased with the equivalent drug concentration of the various nanoparticle formulations, resulting in decreasing cell viability. This is understandable because the larger amount of drug implies that more nanoparticles were incubated with the C6 glioma cells, assuming the drug encapsulation is constant in each nanoparticle. The larger nanoparticle concentration gradient and the presence of endocytic mechanism resulted in higher cytotoxicity. Secondly, it is worthy to note that the Lf-PPN/OX26 and Lf-PPN/OX26+DE2B4 nanoparticle formulation with Lf-PPN conjugation achieved the lowest cell viability among the 3 nanoparticles formulations and the commercial Lf in all equivalent drug concentration levels applied.

Lactoferrin-Coated PPN Cellular Uptake Assay

The exact model of BBB for in vivo delivery of brain examinations was developed with PBCEC to bio mimic the endogenous vascular endothelial cells since it expresses rough protein junctions, as reported by the other studies. The relation between the Lf-PPN cellular uptake affinity proportions was evaluated via ratio between the internalized ratio of the Lf-PPN and the PBCEC conducting with the 1 ng/mL, 2 ng/mL, and 4 ng/mL of free Lf-PPN, Lf-PPN/OX26, and Lf-PPN/OX26+DE2B4 incubation for 2 and 4 hours at 37°C, respectively. In admiration to the Lf-PPN conjugate with the mAbs, the cellular uptake reduced the concentration of immunonanoparticles, predicting a mode of mechanism. The control Lf-PPN cellular uptake via PBCEC is remarkably reduced when

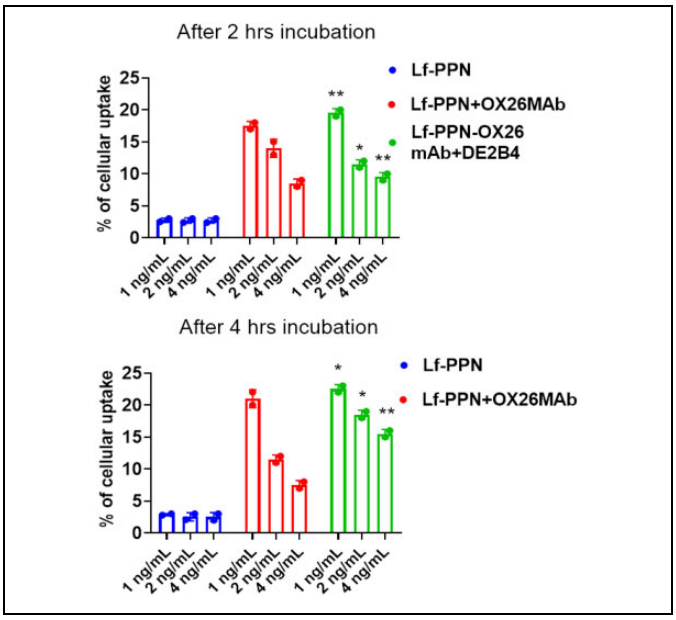

Figure 4. Cellular uptake of Lf-PPN, Lf-PPN/OX26, and Lf-PPN/OX26+DE2B4 incubation for 2 and 4 hours at 37°C. Different concentrations of (1 ng/mL, 2 ng/mL, and 4 ng/mL) PBCECs cellular uptake for 2- and 4-hour incubation time (*P < .05; **P < .01). Lf-PPN indicates lactoferrin-coated PEG-PLA nanoparticles; PBCECs, porcine brain capillary endothelial cells; PEG, polyethylene glycol; PLA, polylactide.

associated with the controlled Lf-PPN (Figure 4).Further, the fluorescence microscopic examinations of the coronal site of the BBC shows certain ratio of Lf-PPN with mAb and are displayed in Figure 5. The enhancing fluorescence intensity in the PBCECs was connected to the increase in the incubation time periods. Later, at 2 ng/mL of Lf-PPN/OX26 incubation with 10, 20, and 30 minutes at 37°C, correspondingly, the remarkable cell accumulation ratio of the dye of Lf-PPN/OX26 in the PBCECs connected with the free Lf-PPN for 1 hour. During initial examinations, we monitored the cellular uptake of Lysotracker (green), free Coumarin (red), and DAPI (blue) and merged (orange) with the Lf-PPN featuring the same ratio of coumarin. Earlier examinations confirmed that the free coumarin dye released from the Lf-PPN denoted very less cellular uptake. Additionally, our outcomes show established stability of coumarin in the Lf-PPN. Hence, we decided that coumarin

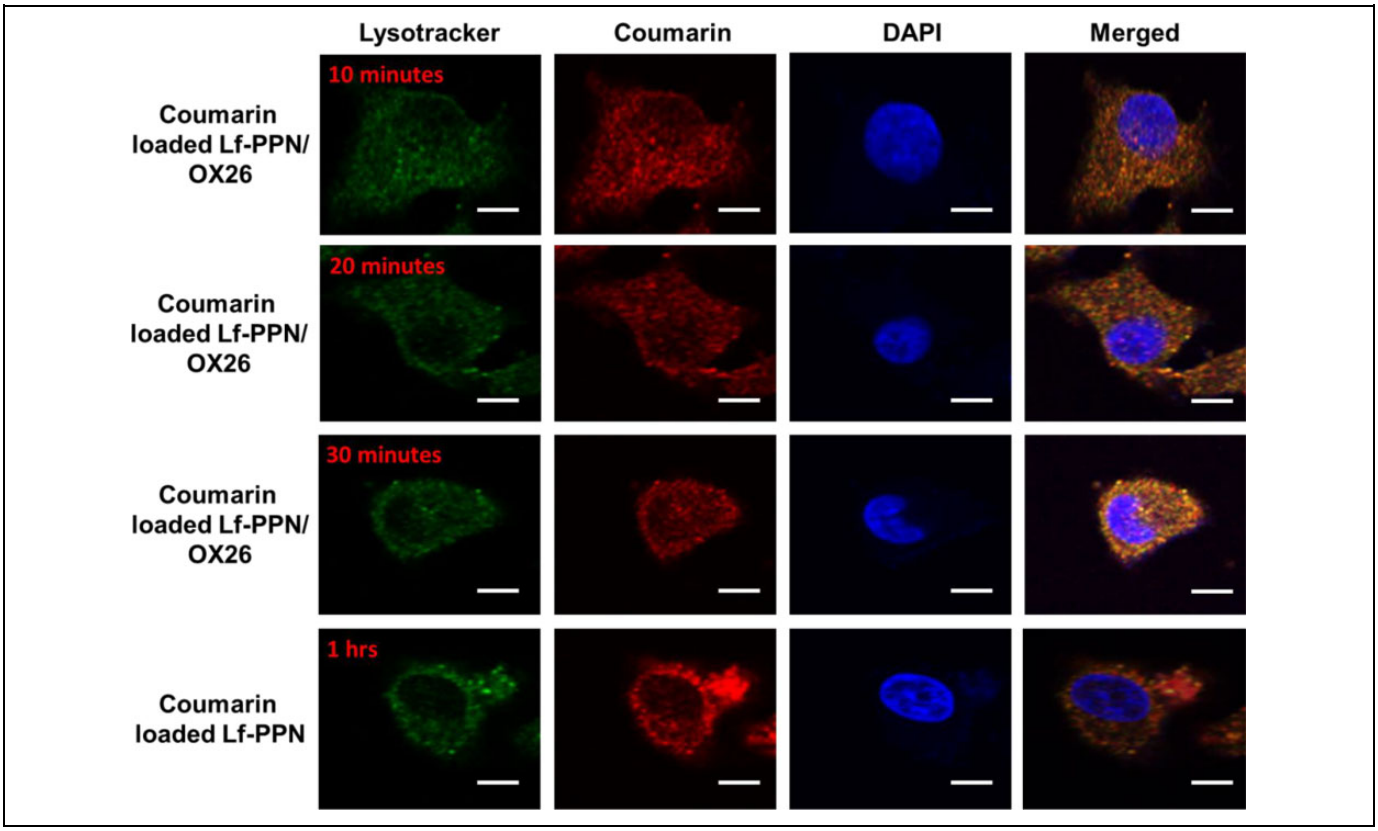

Figure 5. Confocal laser scanning microscopic images of PBCECs after 2 ng/mL of Lf-PPN/OX26 incubation for 10, 20, and 30 minutes at 37°C and without Lf-loaded nanoparticles with 1 hour incubation of Lf-PPN. Lysotracker (green), coumarin (red), DAPI (blue), and merged (orange). Scale bar 10 nm. DAPI indicates 4′,6-diamidino-2-phenylindole; Lf-PPN, lactoferrin-coated PEG-PLA nanoparticles; PBCECs, porcine brain capillary endothelial cells; PEG, polyethylene glycol; PLA, polylactide.

identified in the PBCECs predominantly reflected the Lf-PPN with mAbs.

Toxicity Assay Lf-PPN Conjugate With the mAb to the Tf Receptors

The toxicity of PBCECs of the Lf-PPN was evaluated using PBCEC culture. Later, 2-hour incubation periods with cells were done with the Alamar-Blue solutions at 37°C. The Lf-PPN toxicity in PBCECs was examined and the results are noted in Figure 6. The initial concentrations started at 1 to 4 ng/mL. Furthermore, we examined the Lf-PPN-loaded mAbs in the same cells, which shows less toxicity compared to the free Lf-PPN. These outcomes established that the conjugations of Lf-PPN loaded mAbs delivery process controlled and excellent biocompatibility.

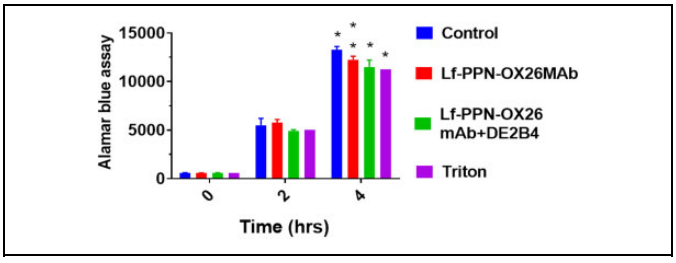

Figure 6. Toxicity effects of Lf-PPN, Lf-PPN-OX26, Lf-PPN-OX26+DE2B4, and 1% triton. The metabolic activity of the PBCECs was calculated with different time periods (0, 2, and 4 hours) by Alamar-Blue assay (*$P < .05$; **$P < .01$). Lf-PPN indicates lactoferrin-coated PEG-PLA nanoparticles; PBCECs, porcine brain capillary endothelial cells; PEG, polyethylene glycol; PLA, polylactide.

Hemolysis Assay of Lf-PPN and Lf-PPN Conjugate With the mAb to the Tf Receptors

The nanoformulations are predictable to interrelate with hRBCs and cause the cell membrane damaging the hemolysis. In order to examine the human health of such adverse effects, in vitro biocompatibility assay was examined. The biocompatibility profiles of RBC caused by the nanoparticles were demonstrated at different concentrations of 5 to 30 µg/mL. Figure 7 displays the dose-dependent hemolytic effect to reduce the toxicity of Lf-PPN, Lf-PPN with OX26, and Lf-PPN with DE2B4 to the Tf receptors. According to the results, Lf-PPN, Lf-PPN with OX26, and Lf-PPN with DE2B4 detected only insignificant hemolysis, which shows extreme biocompatibility for in vivo profiles.

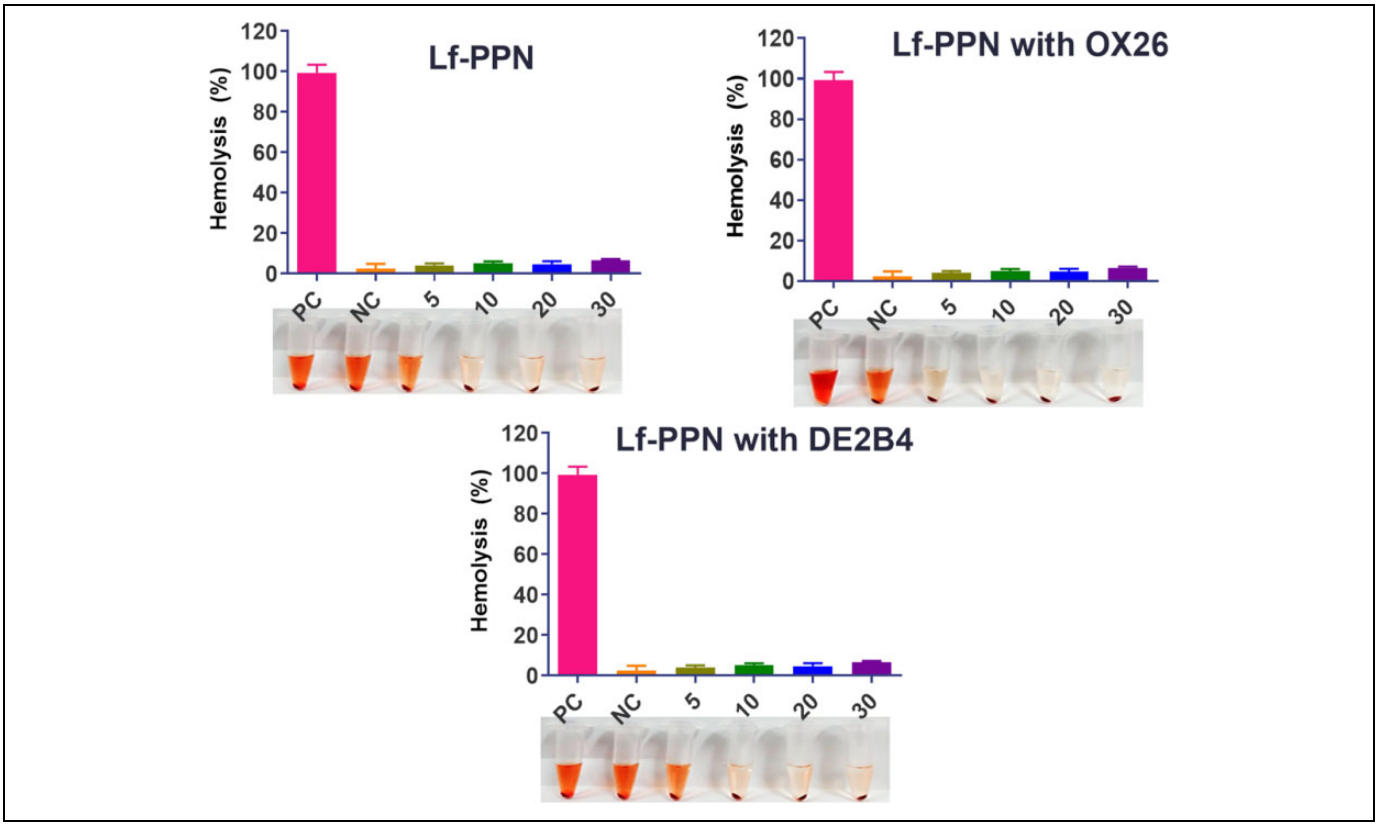

Figure 7. Hemolysis assay with different concentration of Lf-PPN, Lf-PPN with OX26, and Lf-PPN with DE2B4. The result of hemolysis assay reveals the insignificant hemolysis, which shows that it is extremely biocompatible for in vivo profiles (*P < .05; **P < .01). Lf-PPN indicates lactoferrin-coated PEG-PLA nanoparticles; PEG, polyethylene glycol; PLA, polylactide.

Conclusion

The Lf-PPN functionalized with mAbs is the well-established brain delivery receptor by the endothelium to the transport of antiamyloid peptides. We have constructed Lf with PEG-PLA loaded with antiamyloid peptide. The characterization of the TEM and DLS analysis of Lf-PPN show the homogenous distribution with well-organized structures. Also the size of Lf-PPN was less than ~30 nm, the diameters of less than 50 nm is activate for the passive in vivo tumors specific through the EPR effect and can attain the deep penetration of the solid tumors. Also, the size of the loaded antiamyloid peptide was found to be ~20 nm, which is confirmed by the DLS analysis. Further, the cellular uptake results suggested the excellent outcome of Lf-PPN and Lf-PPN encapsulated mAbs in the PBCECs. The mode of mechanism of the Lf-PPN via BBB endothelial cells shows strong evidence of the saturable receptor intercede manner; their cellular uptake ratio tends to reduce with the concentrations. The Lf-PPN is conjugated with antiamyloid peptide from the proteolytic biodegradation and improves their delivery via BBB. Hence, it expects an intracellular cerebral enhance the $iA\beta_5$ concentrations. These types of nanoparticles were used to develop AD treatment in future.

Authors' Note

Guichen Li and Xianghong Sun contributed equally to this work.

Declaration of Conflicting Interests

The author(s) declared no potential conflicts of interest with respect to the research, authorship, and/or publication of this article.

Funding

The author(s) received no financial support for the research, authorship, and/or publication of this article.

ORCID iD

Dongming Wang https://orcid.org/0000-0002-5305-7321

References

1. Oxenkrug G, van der Hart M, Roeser J, Summergrad P. Peripheral tryptophan—kynurenine metabolism associated with metabolic syndrome is different in Parkinson's and Alzheimer's diseases. *Endocrinol Diabetes Metab J*. 2017;1(4). http://europepmc.org/abstract/MED/29292800.
2. Belghali M, Chastan N, Davenne D, Decker LM. Improving dual-task walking paradigms to detect prodromal Parkinson's and Alzheimer's diseases. *Front Neurol*. 2017;8:207. doi:10.3389/fneur.2017.00207.
3. Iadecola C. Vascular and metabolic factors in Alzheimer's disease and related dementias: introduction. *Cell Mol Neurobiol*. 2016;36(2):151-154. doi:10.1007/s10571-015-0319-y.

4. Palma M, Tavakoli S, Brettschneider J, Nichols TE; The Alzheimer's Disease Neuroimaging Initiative. Quantifying uncertainty in brain-predicted age using scalar-on-image quantile regression. 2019. doi:10.1101/853341.
5. Celsi M, Napolioni V, Greicius M, Altmann A; Alzheimer's Disease Neuroimaging Initiative (ADNI); the Alzheimer's Disease Sequencing Project (ADSP). Network propagation of rare mutations in Alzheimer's disease reveals tissue-specific hub genes and communities. 2019. doi:10.1101/781203.
6. Amram S, Iram T, Lazdon E, Vassar R, Porath IB, Frenkel D. Astrocyte senescence in an Alzheimer's disease mouse model is mediated by TGF-β1 and results in neurotoxicity. *BioRxiv*. 2019. doi:10.1101/700013.
7. Milind N, Preuss C, Haber A, et al. Transcriptomic stratification of late-onset Alzheimer's cases reveals novel genetic modifiers of disease pathology. *Biology*. 2019. doi:10.1101/763516.
8. Salama M, Shalash A, Magdy A, et al. Tubulin and tau: possible targets for diagnosis of Parkinson's and Alzheimer's diseases. *PLoS One*. 2018;13(5):e0196436. doi:10.1371/journal.pone.0196436.
9. Williams SM, Schulz P, Sierks MR. Oligomeric α-synuclein and β-amyloid variants as potential biomarkers for Parkinson's and Alzheimer's diseases. *Eur J Neurosci*. 2016;43(1):3-16. doi:10.1111/ejn.13056.
10. Kudo H, Maejima K, Hiruta Y, Citterio D. Microfluidic paper-based analytical devices for colorimetric detection of lactoferrin. *SLAS Technol*. 2020;25(1):2472630319884031. doi:10.1177/2472630319884031.
11. Aasbrenn M, Farup PG, Videm V. Changes in C-reactive protein, neopterin and lactoferrin differ after conservative and surgical weight loss in individuals with morbid obesity. *Sci Rep*. 2019;9:17695. doi:10.1038/s41598-019-54107-z.
12. Khan AI, Liu J, Dutta P. Bayesian inference for parameter estimation in lactoferrin-mediated iron transport across blood-brain barrier. *Biochim Biophys Acta-Gen Sub*. 2020;1864(3):129459. doi:10.1016/j.bbagen.2019.129459.
13. Miranda M, Saccone G, Ammendola A, et al. Vaginal lactoferrin in prevention of preterm birth in women with bacterial vaginosis. *J Maternal-Fetal Neonatal Med*. 2019;1-5. doi:10.1080/14767058.2019.1690445.
14. Hu K, Li J, Shen Y, et al. Lactoferrin-conjugated PEG-PLA nanoparticles with improved brain delivery: in vitro and in vivo evaluations. *J Control Release*. 2009;134:55-61.
15. Velliyagounder K, Rozario SD, Fine DH. The effects of human lactoferrin in experimentally induced systemic candidiasis. *J Med Microbiol*. 2019;68(12):1802-1812. doi:10.1099/jmm.0.001098.
16. Andrés MT, Zaldívar MA, Seisdedos JG, Fierro JF. Cytosolic acidification is the first transduction signal of lactoferrin-induced regulated cell death pathway. *Int J Mol Sci*. 2019;20(23):pii:E5838. doi:10.3390/ijms20235838.
17. Vergara D, Shene C.Encapsulation of lactoferrin into rapeseed phospholipids based liposomes: optimization and physicochemical characterization. *J Food Eng*. 2019;262:29-38. doi:10.1016/j.jfoodeng.2019.05.012.
18. Nowier AM, Darwish HR, Ramadan SI, Othman OE. Polymorphism of lactoferrin gene in Egyptian goats and its association with milk composition traits in Zaraibi breed. *Trop Anim Health Prod*. 2019; doi:10.1007/s11250-019-02099-3.
19. Järemo P, Jejcic A, Jelic V, et al. Erythrocyte amyloid beta peptide isoform distributions in Alzheimer and mild cognitive impairment. *Curr Alzheimer Res*. 2019;16(11):1050-1054. doi:10.2174/1567205016666191010104355.
20. Kucheryavykh LY, Ortiz Rivera J, Kucheryavykh YV, Zayas Santiago A, Diaz Garcia A, Inyushin MY. Accumulation of innate amyloid beta peptide in glioblastoma tumors. *Int J Mol Sci*. 2019;20(10):piiE2482. doi:10.3390/ijms20102482.
21. Zhang Z, Wang X, Pan Y, Wang G, Mao G. The degraded polysaccharide from pyropia haitanensis represses amyloid beta peptide-induced neurotoxicity and memory in vivo. *Int J Biol Macromol*. 2019;146:725-729. doi:10.1016/j.ijbiomac.2019 09.243.
22. Ntarakas N, Ermilova I, Lyubartsev AP. Effect of lipid saturation on amyloid-beta peptide partitioning and aggregation in neuronal membranes: molecular dynamics simulations. *Eur Biophys J*. 2019;48(8):813-824. doi:10.1007/s00249-019-01407-x.
23. Thu TTM, Co NT, Tu LA, Li MS. Aggregation rate of amyloid beta peptide is controlled by beta-content in monomeric state. *J Chem Phys*. 2019;150(22):225101. doi:10.1063/1.5096379.
24. Ngoc Le HT, Park J, Chinnadayala SR, Cho S. Sensitive electrochemical detection of amyloid beta peptide in human serum using an interdigitated chain-shaped electrode. *Biosens Bioelectron*. 2019;144:111694. doi:10.1016/j.bios.2019.111694.
25. Yang Z, Hi J, Xie J, et al. Large-scale generation of functional mRNA-encapsulating exosomes via cellular nanoporation. *Nat Biomedl Eng*. 2020;4(1):69-83. doi:10.1038/s41551-019-0485-1.
26. Kang C, Sun Y, Zhu J, et al. Delivery of nanoparticles for treatment of brain tumor. *Curr Drug Metab*. 2016;17(8):745-754. doi:10.2174/1389200217666160728152939.
27. Li H, Wang X, Yu H, et al. Combining in vitro and in silico approaches to find new candidate drugs targeting the pathological proteins related to the Alzheimer's disease. *Curr Neuropharmacol*. 2018;16(6):758-768. doi:10.2174/1570159X15666171030142108.
28. Zhang S, Xiao T, Yu Y, et al. The extracellular matrix enriched with membrane metalloendopeptidase and insulin-degrading enzyme suppresses the deposition of amyloid-beta peptide in Alzheimer's disease cell models. *J Tissue Eng Reg Med*. 2019;13(10):1759-1769. doi:10.1002/term.2906.
29. Liu MM, Guo ZZ, Liu H, et al. Paper-based 3D culture device integrated with electrochemical sensor for the on-line cell viability evaluation of amyloid-beta peptide induced damage in PC12 cells. *Biosens Bioelectron*. 2019;144:111686. doi:10.1016/j.bios.2019.111686.
30. Chen LM, Chai KX. Matriptase cleaves the amyloid-beta peptide 1-42 at Arg-5, Lys-16, and Lys-28. *BMC Res Notes*. 2019;12(1):5. doi:10.1186/s13104-018-4040-z.
31. Shyam R, Ren Y, Lee J, et al. Intraventricular delivery of siRNA nanoparticles to the central nervous system. *Mol Ther Nucleic Acids*. 2015;4;e242.
32. Fan S, Zheng Y, Liu X, et al. Curcumin-loaded PLGA-PEG nanoparticles conjugated with B6 peptide for potential use in

Alzheimer's disease. *Drug Delivery*. 2018;25(1):1091-1102. doi: 10.1080/10717544.2018.1461955.
33. Sonvico F, Clementino A, Buttini F, et al. Surface-modified nanocarriers for nose-to-brain delivery: from bioadhesion to targeting. *Pharmaceutics*. 2018;10(1):pii E34 doi:10.3390/pharmaceutics 10010034.
34. Cao Y, Tan YF, Wong YS, Liew MWJ, Venkatraman S. Recent advances in chitosan-based carriers for gene delivery. *Mar Drugs*. 2019;17(6):pii: E381.doi:10.3390/md17060381.
35. de Jong OG, Kooijmans SAA, Murphy DE, et al. Drug delivery with extracellular vesicles: from imagination to innovation. *Acc Chem Res*. 2019;52(7):1761-1770. doi:10.1021/acs.accounts. 9b00109.
36. Yi X, Manickam DS, Brynskikh A, Kabanov AV. Agile delivery of protein therapeutics to CNS. *J Control Release*. 2014;190: 637-663. doi:10.1016/j.jconrel.2014.06.017.
37. Grijalvo S, Alagia A, Jorge AF, Eritja R. Covalent strategies for targeting messenger and non-coding RNAs: an updated review on siRNA, miRNA and antimiR conjugates. *Genes*. 2018;9(2):pii: E74. doi:10.3390/genes9020074.
38. Wang P, Zheng X, Guo Q, et al. Systemic delivery of BACE1 siRNA through neuron-targeted nanocomplexes for treatment of Alzheimer's disease. *J Control Release*. 2018;279:220-233.
39. Hedayati S, Niakousari M, Pour ZM. Production of tapioca starch nanoparticles by nanoprecipitation-sonication treatment. *Int J Biol Macromol*. 2019;143:136-142. doi:10.1016/j.ijbiomac. 2019.12.003.
40. Oehrl A, Schötz R, Haag R. Systematic screening of different polyglycerin-based dienophile macromonomers for efficient nanogel formation through IEDDA inverse nanoprecipitation. *Macromol Rapid Commun*. 2019;41(1): e1900510. doi:10.1002/ marc.201900510.
41. Streck S, Neumann H, Nielsen HM, Rades T, McDowell A. Comparison of bulk and microfluidics methods for the formulation of poly-lactic-co-glycolic acid (PLGA) nanoparticles modified with cell-penetrating peptides of different architectures. *I J Pharm X*. 2019;1:100030. doi:10.1016/j.ijpx.2019.100030.
42. Wang Z, Lu Y. Amorphous FePO4/carbon nanotube cathode preparation via in situ nanoprecipitation and coagulation in a microreactor. *ACS Omega*. 2019;4(12):14790-14799. doi:10.1021/ acsomega.9b01343.
43. Lv Y, He H, Qi J, et al. Visual validation of the measurement of entrapment efficiency of drug nanocarriers, *Int J Pharm*. 2018; 547:395-403. doi:10.1016/j.ijpharm.2018.06.025.
44. Fahmy AM, El Setouhy DA, Habib BA, Tayel SA. Enhancement of transdermal delivery of haloperidol via spanlastic dispersions: entrapment efficiency vs. particle size. *AAPS PharmSciTech*. 2019;20(3):95. doi:10.1208/s12249-019-1306-2.
45. Neto EH, Cabezas SS, Sancenón F, Máñez RM, Oliveira RS. Indirect calculation of monoclonal antibodies in nanoparticles using the radiolabeling process with technetium 99 metastable as primary factor: alternative methodology for the entrapment efficiency. *J Pharm Biomed Anal*. 2018;153:90-94. doi:10.1016/ j.jpba.2018.02.017.
46. da Rocha Neto AC, de O da Rocha AB, Almenar E, Maraschin M, Di Piero RM. Factors affecting the entrapment efficiency of β-cyclodextrins and their effects on the formation of inclusion complexes containing essential oils. *Food Hydrocoll*. 2018; 77(3-4): 509-523. doi:10.1016/j.foodhyd.2017.10.029.
47. Ran C, Chen D, Xu M, Du C, Li Q, Jiang Y. A study on characteristic of different sample pretreatment methods to evaluate the entrapment efficiency of liposomes. *J Chromatogr B Analyt Technol Biomed Life Sci*. (2016);1028:56-62. doi:10.1016/j.jchromb. 2016.06.008.
48. Siddik MAB, Das BC, Weiss L, Dhurandhar NV, Hegde V. A MetAP2 inhibitor blocks adipogenesis, yet improves glucose uptake in cells. *Adipocyte*. 2019;8(1):240-253. doi:10.1080/ 21623945.2019.1636627.
49. Ghavami M, Shiraishi T, Nielsen PE. Cooperative cellular uptake and activity of octaarginine antisense peptide nucleic acid (PNA) conjugates. *Biomolecules*. 2019;9(10):pii:E554. doi:10.3390/ biom9100554.
50. Singh BV, Rani M, Singh J, et al. Identifying the preferred interaction mode of naringin with gold nanoparticles through experimental, DFT and TDDFT techniques: insights into their sensing and biological applications. *RSC Adv*. 2016;6(83):79470-79484. doi:10.1039/C6RA12076H.
51. Brauckmann S, Neidnicht KE, Nagel M, Mayer C, Peters J, Hartmann M. Lipopolysaccharide-induced hemolysis is abolished by inhibition of thrombin generation but not inhibition of platelet aggregation. *Inflammation*. 2019;42(5):1767-1776. doi:10.1007/ s10753-019-01038-6.
52. Subarkhan MKM, Ramesh R. Ruthenium(II) arene complexes containing benzhydrazone ligands: synthesis, structure and antiproliferative activity. *Inorg Chem Front*. 2016;3(3):1245-1255. doi:10.1039/c6qi00197a.
53. Pham CT, Thomas DG, Beiser J. Application of a hemolysis assay for analysis of complement activation by perfluorocarbon nanoparticles. *Nanomedicine*. 2014;10(3):651-660. doi:10.1016/j. nano.2013.10.012.
54. Vu HTH, Streck S, Hook SM, McDowell A. Utilization of microfluidics for the preparation of polymeric nanoparticles for the antioxidant rutin—a comparison with bulk production. *Pharm Nanotechno*. 2019;7(6):469-483. doi:10.2174/221173850 7666191019141049.
55. Musumeci T, Bonaccorso A, De Gaetano F, et al. Ventura, a physico-chemical study on amphiphilic cyclodextrin/liposomes nanoassemblies with drug carrier potential. *J Liposome Res*. 2019;1-10. doi:10.1080/08982104.2019.1682603.
56. Levit SL, Walker RC, Tang C. Rapid, single-step protein encapsulation via flash nanoprecipitation. *Polymers*. 2019;11(9):pii E1406. doi:10.3390/polym11091406.
57. Jara MO, Figueroa JC, Landin M, Morales JO. Finding key nanoprecipitation variables for achieving uniform polymeric nanoparticles using neurofuzzy logic technology. *Drug Deliv Transl Res*. 2018;8:1797-1806. doi:10.1007/s13346-017-0446-8.